

On Embedded Recursive Boundary Smoothing In Topology Optimization With Polygonal Mesh and Negative Masks

Prabhat Kumar
Mechanical Engineering
Indian Institute of Technology Kanpur
Kanpur, India
kprabhat@iitk.ac.in

Anupam Saxena
Mechanical Engineering
Indian Institute of Technology Kanpur
Kanpur, India
anupams@iitk.ac.in

Abstract—Topology optimization with polygonal meshes is promising since checkerboards, point-flexures, layering and islanding like singularities get circumvented by the natural imposition of the geometric, 'edge-connectivity' constraint. However, numerous notches get retained on the boundaries of optimal topologies obtained from polygonal tessellations. Previous efforts on Material Mask Overlay Strategy (MMOS) that used hexagonal cells and negative masks have either ignored boundary smoothing, have used it as a post processing step, or have implemented it between the gradient and stochastic searches. Here, we embed boundary smoothing within each iteration of gradient search permitting true evaluation of the objective and the associated sensitivities for all intermediate topologies. Smoothing is performed in a number of steps (represented by parameter β) by systematically shifting the nodes at the boundaries of the continuum. Consequently, some hexagonal cells get degenerated which necessitates their remodeling into Wachspress pentagonal or quadrilateral finite elements to avoid singularity of the stiffness matrix. Material assignment to each cell is accomplished using the logistic function with high values of the material parameter, α approximating the Heaviside function to yield close to binary solutions. However, initial use of high material parameter destabilizes the MMOS since the design sensitivities approach to zero. For stability, α is increased gradually from 1 to an a priori specified value α_s . Compared to its predecessors, the modified algorithm shows promise in terms of quality of solutions obtained in least possible number of function evaluations.

Keywords – Boundary smoothing; Element conversion; Topology optimization; Binary solutions.

I. PRIOR WORK

Topology optimization is a method to optimize the material layout within the given design domain Ω (Fig. 1). The domain is specified by its input ports, fixed boundaries, and output ports to synthesize, e.g., stiff structures and compliant mechanisms. Positions, magnitudes and directions of the input loads define the state at input ports $\partial\Omega_I$ (Fig. 1). Fixed boundaries $\partial\Omega_F$ (Fig. 1) are defined by the nature of constraints on the boundaries. Output port $\partial\Omega_O$ (Fig. 1)

generally indicates the direction of the desired deformation in case a compliant mechanism is designed. The main objective of topology optimization methods is to achieve well defined boundaries for a single material domain. Topology optimization is usually implemented through finite element method for analysis and optimization techniques to synthesize the desired continuum. To date, many approaches have been proposed for topology optimization. One initial method is the Homogenization method proposed by Bendsoe and Kikuchi [1]. Herein, micro-structure features of the domain control the homogenized properties which are used to determine the behavior of the design space Ω . Other popular methods e.g., SIMP (Solid Isotropic Material with Penalization) [2] employ gradient search processes explicitly. Rectangular cells are used to discretize the design domain. Each cell is assigned a design variable ρ_i . If $\rho_i = 0$, that cell is considered empty (void cell), otherwise if $\rho_i = 1$, the corresponding cell is considered filled with the desired material. The elastic modulus of a cell is approximated as $E_i = \rho_i^n E_0$, where n is the penalization parameter and E_0 is the modulus of elasticity of the material. Here, $n \geq 3$ is used to achieve binary solutions. However, some grey cells still remain in the final solutions. PEAK [3] and SIGMOID [4] are other cell based methods. In these, gradients are computed and the design parameters are adjusted iteratively to achieve close to binary solutions. CAMD (Continuous approximation of material distribution) [5] is a node based method where each node is assigned the design density ρ_i^{node} . Shape functions are used to approximate the density of the cells sampled from those at the nodes. In another node-based approach, Guest [6] uses projection, in which the densities at nodes are projected by fixed length scales. Other alternative gradient search procedure like the level set [7]–[10] and material cloud methods [11] are also proposed. Many previous approaches use the Lagrangian type i.e., triangular and rectangular elements for finite element analysis suffer from checkerboard patterns. These methods may also suffer from other connectivity anomalies (geometrical singularities) like islanding, point flexures and layering.

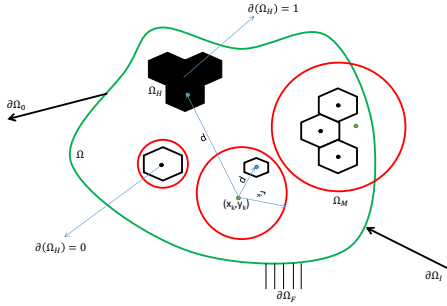


Fig. 1: Implementation of topology optimization with negative masks. Domain (boundary in blue) is shown, discretised with polygonal elements (hex cells) and negative circular masks (circles in red) laid over it. Polygonal mesh ensures that the final topology is free from connectivity singularities like the checkerboard, point-flexure, layering and islanding. Negative circular masks, which are characterized via three parameters (x_i , y_i , and r_i), are used to remove material from beneath. These are the design parameters in the Material Mask Overlay Strategy (MMOS). The number of design variables are reduced compared to SIMP. Polygonal elements, whose centroids are inside a negative circular mask (i.e., $d < r_k$) are modeled as void. The remaining cells are all filled with the desired material. Fixed boundary of the domain, input and output ports are also shown.

Checkerboards overestimate the strain energy and point flexures underestimate the same. The main cause for these geometrical singularities is the presence of single point connections between two diagonally opposite filled rectangular cells [12]. Direct filtering methods [13], [14] or modified algorithms [15]–[17] can alleviate these singularities. To eliminate these unwanted geometrical singularities without additional procedures dedicated for this purpose, honeycomb parametrisation was used [12], [18] since this tessellation gives edge connectivity between any two contiguous cells. These edge connections ensure finite stiffness at all junctions. However, because of the use of hexagonal cells, many V-notches get formed on the boundaries. This work aims at smoothing these boundaries at every stage of the the gradient search. The remainder of the paper is organized as follows. Section II describes a brief about Material Masks Overlay Strategy (MMOS). Section III lays out the boundary smoothing process. Section IV describes element conversion. Section V describes the material modeling. Structure stiff and compliant mechanism problems are described in section VI. Numerical results and discussion are described in section VII. Lastly, we have ended with closure.

II. MATERIAL MASK OVERLAY STRATEGY (MMOS)

The Material Mask Overlay Strategy (MMOS) [19] alleviates geometric singularities and also gives close to binary solutions. MMOS is based on the principle of photo lithography, which allows the removal of material from a group of cells via negative circular masks.

These masks Ω_M (Fig. 1) are termed so because they remove the material beneath them. Three parameters are required to define position and size of each Ω_M . These are the abscissa (x_i) and ordinate (y_i) of the centre, and radius (r_i) of the mask. These variables collectively form

a design vector \mathbf{v} . If K masks are used, the design vector ($\mathbf{v} = (x_i, y_i, r_i), i = 1, \dots, K$) has $3K$ variables. The masks help to reduce the number of design variables compared to SIMP. Ω_M define the material state of Ω implicitly. The density $\rho(x, y)$ of all points (x, y) in the domain Ω with respect to Ω_M is described as follows.

$$\begin{aligned} \rho(x, y) &= 0; \text{ if } (x, y) \subset \text{ any } \Omega_M \\ \rho(x, y) &= 1; \text{ if } (x, y) \not\subset \text{ any } \Omega_M \end{aligned} \quad (1)$$

$\rho(x, y) = 0$ implies that space is void and $\rho(x, y) = 1$ implies that space is filled with the desired material. MMOS uses hexagonal cells to represent the domain. For finite element analysis, a hexagonal cell Ω_H can be further subdivided into six triangular elements [20], two rectangular elements [12], [21], or it can be approximated as a Wachspress hexagonal cell [18], [22]. Cells whose centroids are inside a negative circular mask (i.e., $d < r_k$) (Fig. 1) are modelled as void cells and the remaining ones are filled with the desired material. That is

$$\begin{aligned} \rho(\Omega_H) &= 0; \text{ if } \Omega_H \subset \text{ any } \Omega_M \\ \rho(\Omega_H) &= 1; \text{ if } \Omega_H \not\subset \text{ any } \Omega_M \end{aligned} \quad (2)$$

or,

$$\begin{aligned} \rho(\Omega_H) &= 0; \text{ if } d_k - r_m \leq 0 \quad \forall \Omega_M \\ \rho(\Omega_H) &= 1; \text{ if } d_k - r_m > 0 \quad \forall \Omega_M. \end{aligned} \quad (3)$$

Previous implementations of MMOS [23], [24] are computationally expensive because they use genetic algorithm or alternative stochastic searches. The adaptive MMOS (AMMOS) [25] allows addition and deletion of the masks during optimization process. The performance of circular, elliptical and rectangular masks compared with MMOS suggests that use of circular masks is better [22]. Gradient search is implemented with MMOS in [26].

III. BOUNDARY SMOOTHING

The solutions obtained using the hexagonal tessellation have many V-notches on the exterior and interior boundaries. These notches act as stress concentration regions. Because of these, the continuum subjected to constant multi-axial or harmonic forces, can fail. To smoothen these, i.e., to assuage the notches, boundary smoothing is employed within each iteration of the optimization algorithm of MMOS in [26]. Smooth boundaries help in manufacturing the continuum as well.

Prior works on Material Masks Overlay Strategy (MMOS) have ignored boundary smoothing, used it as a post processing step, or implemented it in between the gradient and stochastic searches [27]. Herein, boundary smoothing is implemented within each iteration of gradient search. Although, this implementation permits true evaluation of the objective and the associated sensitivities for all intermediate topologies, computations can be time

consuming. True evaluation of the objective becomes more important, if deformations are large.

Edges of hexagonal cells along the exterior and interior boundaries are identified. Mid-points of the hexagonal cells on the boundary are joined with straight line segments. Boundary nodes are projected on these respective line segments along the direction of shortest perpendiculars. Modified (new) positions of the nodes are connected for further analysis, without disturbing the original connectivity of the mesh. This process can be performed multiple times to achieve higher levels of smoothing. The number of boundary smoothing steps are represented by parameter β . β can have only integer values ($\beta \in \mathbb{I}$) and can be fixed by the user prior to the analysis or search process. As a consequence of boundary smoothing, some regular hexagonal cells are either modified to irregular cells or get degenerated to pentagonal Ω_P or quadrilateral Ω_Q cells (Fig. 3). It is this degeneration that necessitates their remodeling to avoid singularity in the stiffness matrix.

IV. ELEMENT CONVERSION

Implementation of boundary smoothing affects the nodal positions of regular hexagonal cells. Some nodes of a cell can become collinear. Consecutively, a hexagonal cell can degenerate into a pentagonal or a quadrilateral cell (Fig. 3). Parameter ν_H^{coll} is used to identify, if a hexagonal cell has degenerated to a pentagon or a quadrilateral. $\nu_H^{coll} = 1$ indicates that three consecutive nodes of a hexagonal cell are collinear (Fig. 2a) while $\nu_H^{coll} = 2$ signifies that two groups of three consecutive nodes are collinear (Fig. 2b). The corresponding elements are modified as follows

$$\begin{aligned} \Omega_H &\Rightarrow \Omega_H^{mod}; & \text{if } \nu_H^{coll} &= 0 \\ \Omega_H &\Rightarrow \Omega_P; & \text{if } \nu_H^{coll} &= 1 \\ \Omega_H &\Rightarrow \Omega_Q; & \text{if } \nu_H^{coll} &= 2 \end{aligned} \quad (4)$$

here, Ω_P represents a pentagonal Wachspress finite element and Ω_Q denotes a quadrilateral finite element.

V. MATHEMATICAL MODELLING AND GRADIENT CALCULATIONS

A. Material Modelling

Material assignment is approximated using the logistic function (Fig. 4a), $f(\alpha, t)$ defined below.

$$f(\alpha, t) = \frac{1}{1 + \exp(-\alpha t)} \quad (5)$$

where α is a parameter, which can be selected either prior to the analysis or increased gradually (herein, it is increased gradually with the number of function evaluations (Fig. 4b) to achieve close to binary solutions. t is a variable $\in (-\infty, \infty)$. If $\alpha \rightarrow +\infty$, $f(\alpha, t) \rightarrow H(t)$, where $H(t)$ is the

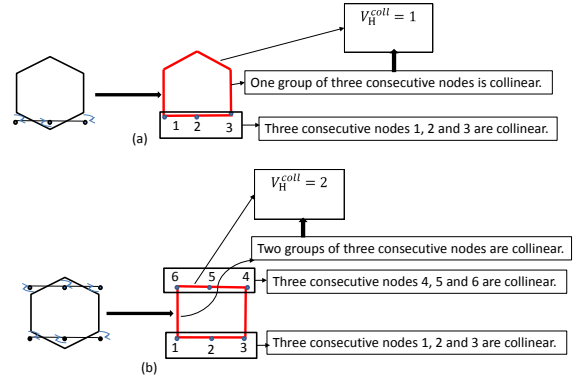


Fig. 2: Degeneration of a hexagonal cell into either a pentagonal cell or quadrilateral cell.

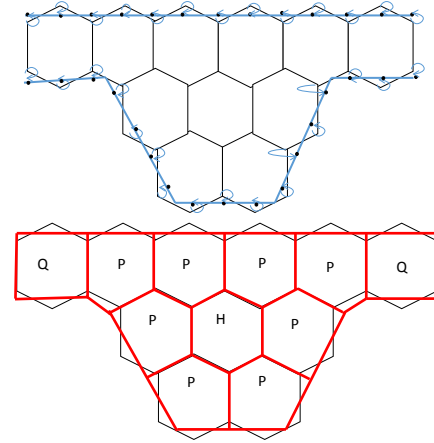


Fig. 3: Many notches are formed on the boundaries due to the use of a hexagonal mesh. Midpoints of all boundary hexagonal cells are joined by straight line segments. Boundary nodes are projected on the respective line segments along the direction of shortest respective perpendiculars. Modified (new) positions of the nodes are used for further analysis without disturbing the original connectivity of the hexagonal cells. This process can be performed multiple times to achieve much smoother contours. The parameter for boundary smoothing is β , the number of boundary smoothing steps. β is fixed prior to the analysis/search process and can only have integer values. Because of smoothing, some hexagonal cells are degenerated into pentagonal or quadrilateral cells, which necessitates their remodeling by using Wachspress finite elements, to avoid the singularity of the stiffness matrix. Boundary smoothing is implemented within each iteration of gradient search permitting true evaluation of the objective and the associated sensitivities for all the intermediate topologies.

Heaveside function defined as follows

$$\begin{aligned} H(t) &= 1, & \forall t &> 0 \\ H(t) &= 0, & \text{otherwise.} \end{aligned} \quad (6)$$

To facilitate topology optimization, variable t is defined to relate all negative masks with the i^{th} cell [26]. The density

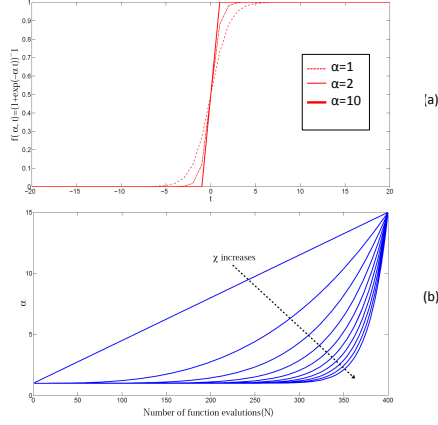


Fig. 4: Material assignment to each polygonal element is accomplished using the logistic function. For high values of the material parameter α , $f(\alpha, t)$ approximates Heaviside function to yield close to the binary topologies. However, initial use of high α destabilizes the topology algorithm since the design sensitivities approach zero quickly. Therefore, α is initially chosen small (≈ 1) and is gradually increased with the number of function evaluations to an a priori specified value α_s .

of the i^{th} cell is defined as.

$$\rho_i = \prod_{j=1}^{M_a} \frac{1}{1 + \exp(-\alpha(d_{ij} - r_j))} + \epsilon \quad (7)$$

where M_a is the number of masks, $d_{ij} = \sqrt{(x_i - x_j)^2 + (y_i - y_j)^2}$ is the distance between the centres of Ω_M and the centroid (x_i, y_i) of the i^{th} cell, and r_j is the radius of Ω_M . For large α

$$\begin{aligned} \rho_i &\approx 0, \text{ if any } d_{ij} < r_j \text{ or } \Omega_H \subset \Omega_M \\ \rho_i &\approx 1, \text{ if all } d_{ij} > r_j \text{ or } \Omega_H \not\subset \Omega_M. \end{aligned} \quad (8)$$

and irrespective of the value of α

$$\rho_i = \frac{1}{2}, \text{ if } d_{ij} = r_j \text{ for some } \Omega_M \text{ and } \Omega_H \notin \text{all other } \Omega_M \quad (9)$$

Equation (9) suggests that cells whose centroids lie very near or on the boundary of masks, are grey, neither fully void nor fully solid. Hence, such cells are assigned fictitious material states. To ensure non-singularity of the global stiffness matrix in the analysis, a small term $\epsilon > 0$ is introduced in (7).

As mentioned previously, for stability of the MMOS, α is varied as follows.

$$\alpha = 1 + (\alpha_s - 1) \left(\frac{N}{N_{max}} \right)^\chi \quad (10)$$

where α_s is an a priori specified value ($\approx c$), N is current function evaluation number, N_{max} is maximum number of function evaluations and χ is a user chosen parameter.

B. Gradient Calculation

The material layout of the continuum is determined via locations and sizes of the negative masks. These parameters

change as gradient search progresses. To derive the search, design sensitivities are needed with respect to design vector $\mathbf{v} = (x_i, y_i, r_i), i = 1, \dots, K$. These gradients are calculated analytically as follows. Let $f_0(\mathbf{v})$ represent either the objective or constraint relation. Then

$$\frac{\partial f_0}{\partial \eta_k} = \sum_{H_6=1}^{N_H} \left\{ \frac{\partial f_0}{\partial \rho_j} \right\} \left\{ \frac{\partial \rho_j}{\partial \eta_k} \right\} \quad (11)$$

where N_H is the number of the hexagonal cells and η_k represents x_m, y_m or r_m for Ω_M . Expressions for $\frac{\partial \rho_j}{\partial \eta_k}$, i.e., $\frac{\partial \rho_j}{\partial x_m}, \frac{\partial \rho_j}{\partial y_m}$ and $\frac{\partial \rho_j}{\partial r_m}$ are obtained as

$$\frac{\partial \rho_j}{\partial x_m} = \rho_j \left[\frac{\alpha \exp\{-\alpha(d_{jm} - r_m)\}}{1 + \exp\{-\alpha(d_{jm} - r_m)\}} \right] \left[\frac{x_m - x_j}{d_{jm} + \delta} \right] \quad (12)$$

$$\frac{\partial \rho_j}{\partial y_m} = \rho_j \left[\frac{\alpha \exp\{-\alpha(d_{jm} - r_m)\}}{1 + \exp\{-\alpha(d_{jm} - r_m)\}} \right] \left[\frac{y_m - y_j}{d_{jm} + \delta} \right] \quad (13)$$

$$\frac{\partial \rho_j}{\partial r_m} = -\rho_j \left[\frac{\alpha \exp\{-\alpha(d_{jm} - r_m)\}}{1 + \exp\{-\alpha(d_{jm} - r_m)\}} \right]. \quad (14)$$

For the existence and uniqueness of $\frac{\partial \rho_j}{\partial x_m}$ and $\frac{\partial \rho_j}{\partial y_m}$ when $d_{jm} = 0$ a small $\delta > 0$ is introduced in the above equations [26].

VI. FORMULATION FOR OPTIMAL STIFF STRUCTURES AND COMPLIANT MECHANISMS

Topology optimization of stiff structures (Fig. 5a and Fig. 5b) and compliant mechanisms (Fig. 5c) can be formulated as constraint optimization problems. A standard formulation of stiff structures involves minimization of strain energy (SE) subjected to the volume constraint. Mathematically, in the discrete setting

$$\begin{aligned} \text{Minimise : } SE(\boldsymbol{\rho}) &= \frac{1}{2} \mathbf{U}^T \mathbf{K} \mathbf{U} \\ \text{Subjected to : } V &= \sum_{i=1}^{N_c} \rho_i \leq V^0 \end{aligned} \quad (15)$$

where $\boldsymbol{\rho} = \rho_i$ represents cell densities, and V and V^0 represent volume fraction and its upper limit respectively. \mathbf{K} is the intermediate global stiffness matrix and \mathbf{U} is the corresponding overall displacement (from finite element computation) of the design domain. From equilibrium, $\mathbf{F} = \mathbf{K} \mathbf{U}$. Boundary smoothing is implemented in each iteration, due to which the affected hexagonal cells are converted into pentagonal or quadrilateral cells. To find the stiffness matrix of the i^{th} cell, it is needed to identify its type. $\mathbf{k}_i = \rho_i \mathbf{k}^0$ is calculated and then the global stiffness matrix \mathbf{K} is assembled, where \mathbf{k}^0 is the stiffness of the corresponding solid cell. Depending upon the type of the i^{th} cell, the corresponding local stiffness matrix is of different size. That is for a hexagonal cell size of \mathbf{k}_i is 12×12 , while for a pentagonal or quadrilateral cells they are 10×10 and 8×8 respectively. Finite element method is employed to determine the overall intermediate displacement \mathbf{U} . Nodal displacements \mathbf{u}_i for each cell are

extracted.

Gradient of the strain energy (SE) with respect to the cell densities is calculated as:

$$\frac{\partial SE(\boldsymbol{\rho})}{\partial \rho_i} = -\frac{1}{2} \mathbf{u}_i \frac{\partial \mathbf{k}_i}{\partial \rho_i} \mathbf{u}_i \quad (16)$$

The derivative of strain energy (SE) with respect to a design variable η_k is calculated by using chain rule, from (11)

$$\frac{\partial SE(\boldsymbol{\rho})}{\partial \eta_k} = \sum_{j=1}^{N_c} \left(\frac{\partial SE(\boldsymbol{\rho})}{\partial \rho_j} \frac{\partial \rho_j}{\partial \eta_k} \right). \quad (17)$$

where $\frac{\partial \rho_j}{\partial \eta_k}$ are given in (12-14).

The flexibility-stiffness multi-criteria objective [31], which maximises the desired output deformation and minimises the internal energy to obtain optimal continuum can be stated as

$$\begin{aligned} \text{Minimise : } & - \left[\frac{MSE(\boldsymbol{\rho})}{SE(\boldsymbol{\rho})} \right] = -p \left[\frac{\mathbf{V}^T \mathbf{K} \mathbf{U}}{\frac{1}{2} \mathbf{U}^T \mathbf{K} \mathbf{U}} \right] \\ \text{Subjected to : } & V = \sum_{i=1}^{N_c} \rho_i \leq V^0 \end{aligned} \quad (18)$$

Here, \mathbf{V} is the displacement due to a dummy unit force, applied in the direction of the desired deformation [32]. Mutual strain energy (MSE), which is equal to desired deformation, is calculated by using the virtual work principle. For \mathbf{F}_d as the dummy load vector, $\mathbf{F}_d = \mathbf{K} \mathbf{V}$. Displacements \mathbf{V} are calculated using finite element method. p is scaling constant. Gradient of the mutual strain-energy with respect to densities can be computed as

$$\frac{\partial MSE(\boldsymbol{\rho})}{\partial \rho_i} = -(\mathbf{v}_i^T) \frac{\partial \mathbf{k}_i}{\partial \rho_i} \mathbf{u}_i \quad (19)$$

To determine the derivative of the objective in (18) with respect to the design parameter

$$\frac{\partial}{\partial \eta_j} \left(- \frac{MSE(\boldsymbol{\rho})}{SE(\boldsymbol{\rho})} \right) = - \frac{\frac{\partial}{\partial \eta_j} MSE(\boldsymbol{\rho})}{SE(\boldsymbol{\rho})} - \frac{MSE(\boldsymbol{\rho}) \frac{\partial}{\partial \eta_j} SE(\boldsymbol{\rho})}{[SE(\boldsymbol{\rho})]^2} \quad (20)$$

To find the right hand side of (20), the following chain rule is employed.

$$\frac{\partial}{\partial \eta_j} MSE(\boldsymbol{\rho}) = \sum_{i=1}^{N_c} \left(\frac{\partial MSE(\boldsymbol{\rho})}{\partial \rho_i} \frac{\partial \rho_i}{\partial \eta_j} \right) \quad (21)$$

VII. NUMERICAL RESULTS AND DISCUSSION

A. Numerical Results

Three design optimization problems are solved. The first problem (Fig. 5a) involves designing a stiff beam under a single constant load, which is applied at the centre of the lower edge of the beam. Following parameters are used to achieve the solution (Fig. 6). Mesh size of (60×30) cells, boundary smoothing steps $\beta = 8$, a priori specified

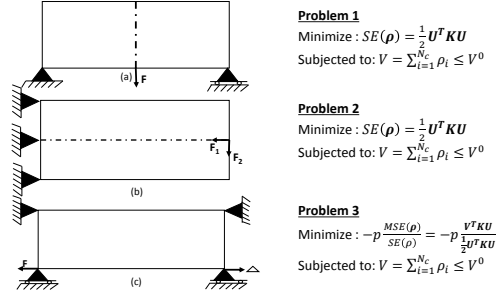


Fig. 5: Classical problems in stiff structure (problems 1-2) and compliant mechanism (problem 3). Bold arrows represent the applied loads and the direction of desired deformation Δ . Boundaries constraints are also shown.

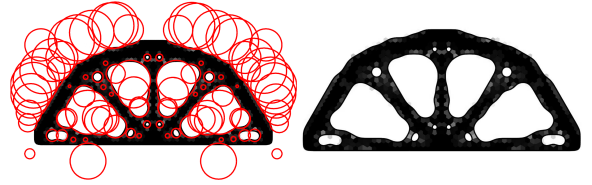


Fig. 6: Topology optimized solution with boundary smoothing of problem 1 is shown. Solution is shown with (left) and without (right) negative circular masks.

value of α , $\alpha_s = 5$, number of masks in the horizontal direction $N_x = 10$, number of masks in the vertical direction $N_y = 10$, volume fraction $V^0 = 0.25$, elastic modulus $E = 100$ MPa, maximum radius (r_i) of the masks $R_{max} = 10$ mm, thickness $t = 1$ mm, poison's ration $\mu = 0.30$, $\chi = 2$ and applied force $\mathbf{F} = -30$ N. Solution is generated within 150 iterations and 300 function evaluations.

The second problem (Fig. 5b) involves designing of a stiff beam under multi-loads, which are applied at the centre of the rightmost edge of the beam. Following parameters are used to achieve the solution (Fig. 7). Mesh size of (50×31) cells, boundary smoothing steps $\beta = 10$, a priori specified value of α , $\alpha_s = 4$, number of masks in the horizontal direction $N_x = 10$, number of masks in the vertical direction $N_y = 12$, volume fraction $V^0 = 0.20$, elastic modulus $E = 1000$ MPa, maximum radius (r_i) of the masks $R_{max} = 14$ mm, thickness $t = 1$ mm, poison's ration $\mu = 0.30$, $\chi = 2$ and applied force $\mathbf{F} = -20$ N. The solution is generated within 70 iterations and 130 function evaluations.

The third problem (Fig. 5c) involves designing of a compliant inverter mechanism under a single constant load applied at the lower leftmost edge of the inverter. Following parameters are used to achieve the solution. Mesh size of (40×20) cells, boundary smoothing steps $\beta = 4$, a priori specified value of α , $\alpha_s = 4$, number of masks in the horizontal direction $N_x = 10$, number of masks in the vertical direction $N_y = 12$, volume fraction $V^0 = 0.20$, elastic modulus $E = 1000$ MPa, maximum radius (r_i) of

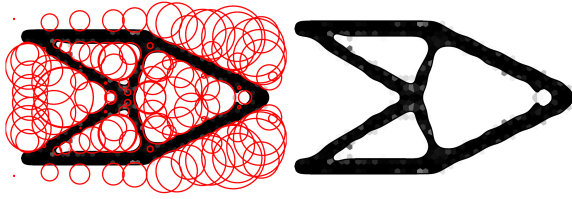


Fig. 7: Topology optimized solution with boundary smoothing of problem 2 is shown. Solution is shown with (left) and without (right) negative circular masks.

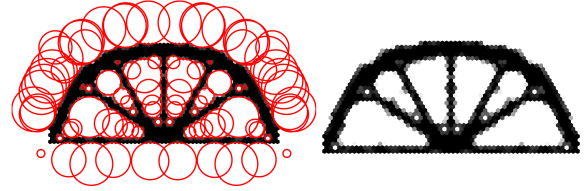


Fig. 10: Topology optimized solution without boundary smoothing of problem 1 is shown. Solution is shown with (left) and without (right) negative circular masks.

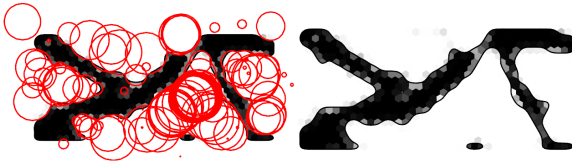


Fig. 8: Topology optimized solution with boundary smoothing of problem 3 is shown. Solution is shown with (left) and without (right) negative circular masks.

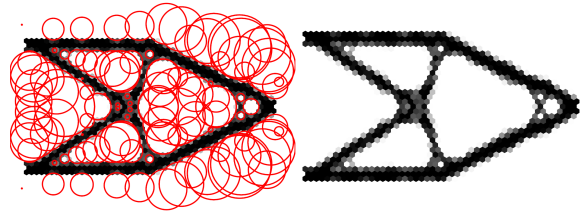


Fig. 11: Topology optimized solution without boundary smoothing of problem 2 is shown. Solution is shown with (left) and without (right) negative circular masks.

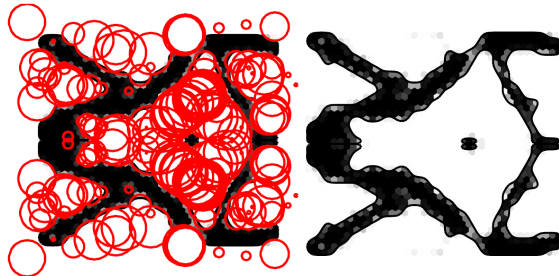


Fig. 9: Topology optimized complete solution with boundary smoothing of problem 3 is shown. Solution is shown with (left) and without (right) negative circular masks.

the masks $R_{max} = 20/3$ mm, thickness $t = 1$ mm, poisson's ration $\mu = 0.30$, $\chi = 2$ and applied force $\mathbf{F} = -40$ N. The symmetric half solution (Fig. 8) and complete solution (Fig. 9) are generated within 300 function evaluations.

During the search process in all problems, β is kept constant and chosen prior to the sequence of analysis. However, for calculation of the objective and its derivative, the value of α is varied gradually from 1 to its an a priori specified value with the iteration. For volume constraint and its derivative, α is kept constant ($=1$).

B. Discussion

Our focus is to achieve smooth boundaries along with close to optimal binary solutions. Smoothness of the

boundary of the topology seems to depend upon the β , the number of smoothing steps ($\subset I$). Close to binary solutions can be achieved with larger α . However, large α will lead to numerical instability because most derivatives in equations (12-14) tend to zero. Therefore, α is varied gradually with the iterations from 1 to an a priori specified value α_s . This variation maintains small $\alpha \approx 1$ in the initial stages of the algorithm.

1) *Observations from solutions:* In all solutions, checkerboards are not observed. This is because of the virtue of the geometry associated with the hexagonal tessellation. In all problems which have symmetric loading and boundary conditions, optimized solutions are such that, masks are symmetric, due to which the final continuum is also symmetric. The contour of the solutions are smooth and solutions are close to binary. Solutions with $\beta = 0$, i.e., when no smoothing is employed, are presented in [26] and reproduced in (Fig. 10 to Fig. 13) for purpose of comparison. Solutions in (Fig. 6 to Fig. 9) have grey cells on their boundaries. This is expected since the centroids of the boundary cells are very close to the mask perimeters. In (Fig. 8), presence of a small island is observed. Per [26] the strain energy associated with this region is close to zero.

VIII. CLOSURE

In the proposed new approach, boundary smoothing is embedded with MMOS [26], in each iteration of the gradient search process. The smoothness of the boundaries

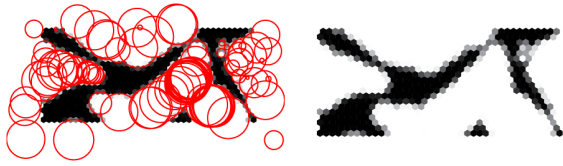


Fig. 12: Topology optimized solution without boundary smoothing of problem 3 is shown. Solution is shown with (left) and without (right) negative circular masks.

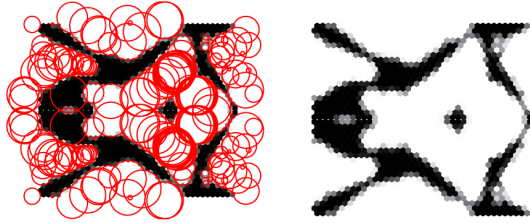


Fig. 13: Topology optimized complete solution without boundary smoothing of problem 3 is shown. Solution is shown with (left) and without (right) negative circular masks.

is associated with $\beta (\subset I)$, which is selected by the user prior to the analysis. Implementation of boundary smoothing in each iteration permits true evaluation of the objective and sensitivities. Close to binary solutions are obtained by increasing α gradually with iterations from 1 to an a priori specified value. Numerical instability is avoided by keeping α close to 1 during the initial stages in optimization. Detailed investigation on the proposed boundary smoothing approach are planned for the near future.

REFERENCES

- [1] Bendsoe D., Kikuchi D. "Generating optimal topologies in structural design using a homogenization method." *Comput Methods Appl Mech Eng* 1988; 71(2):197224
- [2] Bendse MP. "Optimization of Structural Topology, Shape and Material." Springer: Berlin, 1995.
- [3] Yin L., Ananthasuresh GK. "Topology optimization of compliant mechanisms with multiple materials using a peak function material interpolation scheme." *Structural and Multidisciplinary Optimization* 2001; 23:4962.
- [4] Saxena R., Saxena A. "On honeycomb representation and sigmoid material assignment in optimal topology synthesis of compliant mechanisms." *Finite Elements in Analysis and Design* 2007; 43(14):10821098.
- [5] Matsui K., Terada K. "Continuous approximation of material distribution for topology optimization." *Int J Numer Methods Eng* 2004; 59:19251944
- [6] Guest JK, Prvost JH, Belytschko T. "Achieving minimum length scale in topology optimization using nodal design variables and projection functions." *International Journal for Numerical Methods in Engineering* 2004; 61:238254.
- [7] Sethian, J.A., and Wiegmann, A. "Structural boundary via level set and immersed interface methods." *Journal of Computational Physics* 200; 163 (2), pp. 489528.
- [8] Luo, J.Z., Luo, Z., Chen, S. K., Tong, L. Y., Wang. M. Y. "A new level set method for systematic design of hinge-free compliant mechanisms." *Computational Methods in Applied Mechanics in Engineering* 2008; 198, pp. 318-331.
- [9] Wang, M. Y., Chen, S.K., Wang, X.M., Mei. . Y.L. "Design of multi-material compliant mechanisms using level set methods." *Journal of Mechanical Design* 2005; 127, pp. 941-956.
- [10] Jiang, C., and Jia, H. "Evolutionary Based Intelligent Algorithm for Topology Optimization of Structure." *Proceedings of the Sixth International Conference on Intelligent Systems Design and Applications (ISDA'06)*, 897 -902
- [11] Chang, S. Y., and Youn, S. K. "Material cloud methods mathematical investigation and numerical application for 3D engineering design." *International Journal of Solids and Structures* 2006; 43 (17), pp 5337-5354.
- [12] Saxena R, Saxena A. "On honeycomb parameterization for topology optimization of compliant mechanisms." *ASME Design Engineering Technical Conferences, Design Automation Conference, Chicago, IL , DETC2002/DAC-48806, September 2003.*
- [13] Sigmund, O. "Design of Material Structures using Topology Optimization." *DCAMM Report S.69, Department of Solid Mechanics, Ph. D. thesis 1994, DTU, Denmark.*
- [14] Sigmund O. "Morphology-based black and white filters for topology optimization." *Structural and Multidisciplinary Optimization* 2007; 33:401424.
- [15] Poulsen, T. A. "A new scheme for imposing minimum length scale in topology optimization." *International Journal for Numerical Methods in Engineering* 2003; Vol. 57, pp. 741 -760.
- [16] Yoon, G., Kim, Y., Bendsoe, M., Sigmund, O. "Hinge-free topology optimization with embedded translation-invariant differentiable wavelet shrinkage." *Structural and Multidisciplinary Optimization* 2004; 27, 139150.
- [17] Rahmatalla, S., Swan, C.C. "Sparse monolithic compliant mechanisms using continuum structural topology optimization." *International Journal for Numerical Methods in Engineering* 2005; 62, 15791605.
- [18] Talischi C, Paulino GH, Le Chau H. "Honeycomb Wachspress finite elements for structural topology optimization." *Structural and Multidisciplinary Optimization* 2009; 37(6):569583.
- [19] Saxena A. "A Material-Mask Overlay Strategy for Continuum Topology Optimization of Compliant Mechanisms using Honeycomb Discretization." *ASME Journal of Mechanism Design* 2009, 130 (8), DOI:10.1115/1.2936891
- [20] Langelaar M. "The use of convex uniform honeycomb tessellations in structural topology optimization." In: *Proceedings of the 7th world congress on structural and multidisciplinary optimization*. Seoul, South Korea, 2125 May 2007
- [21] Saxena R, Saxena A. "On honeycomb representation and sigmoid material assignment in optimal topology synthesis of compliant mechanisms." *Finite Elements in Analysis and Design* 2007; 43(14):10821098.
- [22] Saxena A. "On an adaptive mask overlay topology synthesis method." *ASME Design Engineering and Technical Conferences, Montreal, Canada, 1518 Aug 2009, DETC2010-29113*
- [23] Saxena A. "A material-mask overlay strategy for continuum topology optimization of compliant mechanisms using honeycomb discretization." *ASME Journal of Mechanism Design* 2009; 130(8):082304:19. DOI: 10.1115/1.2936891.
- [24] Jain C, Saxena A. "An improved material-mask overlay strategy for topology optimization of structures and compliant mechanisms." *ASME Journal of Mechanism Design* 2010; 132(6):061006:110. DOI: 10.1115/1.4001530.

- [25] Saxena A. "An adaptive material mask overlay method: modifications and investigations on binary, well connected robust compliant continua." *ASME Journal of Mechanism Design* 2011; 133(4):041004:111. DOI: 10.1115/1.4003804.
- [26] Saxena A. "Topology optimization with negative masks using gradient search." *Structural and Multidisciplinary Optimization* 2011; 44(5):629649.
- [27] Saxena A., Sauer A. "Combined gradient-stochastic optimization with negative circular masks for large deformation topologies." *Int. J. Numer. Meth. Engng* 2013; 93:635663
- [28] Wachspress EL. "Rational Finite Element Basis." Academic Press: New York, NY, 1975.
- [29] Sukumar N, Tabarraei A. "Conforming polygonal finite elements." *International Journal for Numerical Methods in Engineering* 2004; 61(12):20452066.
- [30] Dasgupta G. "Interpolants within convex polygons: Wachspress shape functions." *Journal of Aerospace Engineering* 2003; 16. DOI: 10.1061/(ASCE)08931321(2003)16:1(1).
- [31] Saxena A, Ananthasuresh GK. "On an optimality property of compliant topologies." *Struct Multidisc Optim* 2000; 19: 3649
- [32] Yin L, Ananthasuresh GK. "Design of distributed compliant mechanisms." *Mech Based Des Struct Mach* 2003; 31(2):151179